Supplementary Information
Modelling of earthquake swarms suggests magmatic fluids in the upper crust beneath the Eger Rift

Pınar Büyükakpınar[1*], Torsten Dahm[1,2], Sebastian Hainzl[1,2], Marius Isken[1], Matthias Ohrnberger[2], Jana Doubravová[3], Siegfried Wendt[4], Sigward Funke[5]

[1*]Physics of Earthquakes and Volcanoes, GFZ Helmholtz Centre for Geosciences, Potsdam, Germany.
[2]Institute for Earth and Environment, University of Potsdam, Potsdam, Germany.
[3]Institute of Geophysics, Czech Academy of Sciences, Prague, Czech Republic.
[4]Geophysical Observatory Collm, Institute for Earth System Science and Remote Sensing, Leipzig University, Leipzig, Germany.
[5]Institute for Earth System Science and Remote Sensing, Leipzig University, Leipzig, Germany.

*Corresponding author(s). E-mail(s): pinar@gfz.de;
Contributing authors: torsten.dahm@gfz.de; hainzl@gfz.de; isken@gfz.de; Matthias.Ohrnberger@geo.uni-potsdam.de; doubravka@ig.cas.cz; wendt@rz.uni-leipzig.de; sfunke@uni-leipzig.de;

The Supplementary Information includes nine additional figures (Figs. S1 and S9) and one table (Table S1), which offer more details and support the interpretations in the main article.

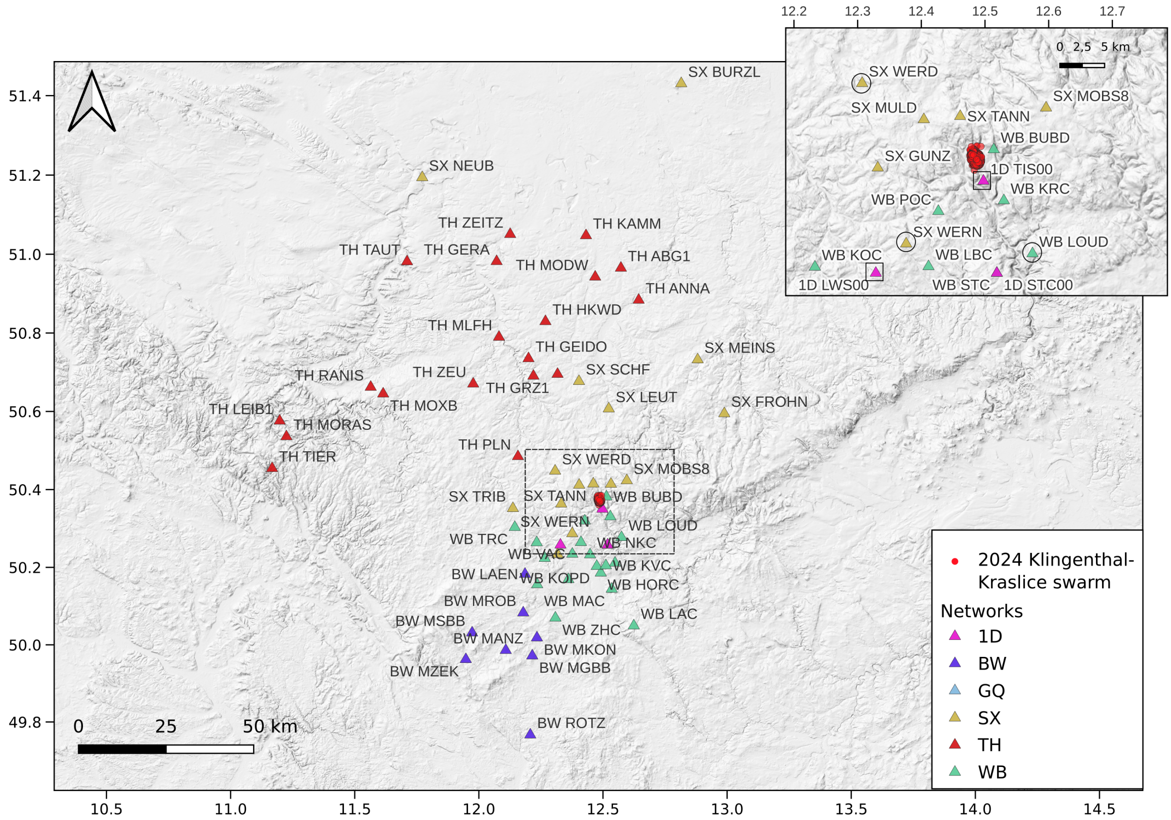

Fig. S1: Map of seismic stations that recorded the 2024 Klingenthal–Kraslice swarm (red circles), labeled in NET.STA format. The inset shows a zoomed-in view highlighting closely spaced stations. Black circles indicate the stations used in the V_P/V_S calculations (see the Methods section in the main article), while rectangles mark borehole stations used for spectral analysis (see Figure S8). Waveform data were sourced from borehole arrays operated by the ICDP (Drilling the Eger Rift) 1D network (Longterm monitoring of swarm earthquakes in the western Eger rift; GFZ Potsdam; [1]) together with surface stations from WB [2, 3], SX [4], TH [5], BW [6], and the GQ networks [7]. See the Data Availability section in the main article.

Table S1: List of seismic stations used in this study, including their network codes, names, geographic coordinates, and elevations.

No	Network	Station	Latitude (°)	Longitude (°)	Elevation (m)
1	1D	LWSA2	50.25804	12.32845	617
2	1D	LWS00	50.25801	12.32852	617
3	1D	STC00	50.25805	12.51853	688
4	1D	TIS00	50.35028	12.49744	700
5	BW	LAEN	50.18281	12.18586	675
6	BW	MANZ	49.98620	12.10830	635
7	BW	MGBB	49.97196	12.21497	650
8	BW	MKON	50.01864	12.23383	614
9	BW	MROB	50.08315	12.17859	570
10	BW	MSBB	50.03143	11.97277	622
11	BW	MZEK	49.96259	11.94743	627
12	BW	ROTZ	49.76690	12.20700	430
13	GQ	LNDWU	50.25793	12.32901	630
14	SX	BURZL	51.43052	12.81501	214
15	SX	FROHN	50.59483	12.98856	483
16	SX	GUNZ	50.36350	12.33160	669

No	Network	Station	Latitude (°)	Longitude (°)	Elevation (m)
17	SX	LEUT	50.60720	12.52309	411
18	SX	MEINS	50.73247	12.88118	501
19	SX	MOBS7	50.41433	12.53191	750
20	SX	MOBS8	50.42344	12.59578	906
21	SX	MULD	50.41180	12.40390	693
22	SX	NEUB	51.19420	11.77190	200
23	SX	ROHR	50.23400	12.31700	629
24	SX	SCHF	50.67720	12.40310	384
25	SX	TANN	50.41500	12.46100	836
26	SX	TRIB	50.35200	12.13700	510
27	SX	WERD	50.44800	12.30700	596
28	SX	WERN	50.28740	12.37610	672
29	TH	ABG1	50.96532	12.57208	247
30	TH	ANNA	50.88399	12.64365	249
31	TH	FRAU	50.69544	12.31685	362
32	TH	GEIDO	50.73530	12.19990	346
33	TH	GERA	50.98203	12.07150	277
34	TH	GRZ1	50.69080	12.21964	401
35	TH	HKWD	50.82970	12.26811	313
36	TH	KAMM	51.04760	12.43147	179
37	TH	LEIB1	50.57607	11.19780	451
38	TH	MLFH	50.78982	12.08091	220
39	TH	MODW	50.94269	12.46844	242
40	TH	MORAS	50.53608	11.22470	618
41	TH	MOXB	50.64523	11.61447	409
42	TH	PLN	50.48520	12.15730	432
43	TH	RANIS	50.66236	11.56432	383
44	TH	TAUT	50.98161	11.71074	331
45	TH	TIER	50.45468	11.16721	698
46	TH	ZEITZ	51.05070	12.12605	158
47	TH	ZEU	50.67064	11.97713	331
48	WB	BUBD	50.38174	12.51362	745
49	WB	HOPD	50.22378	12.26547	731
50	WB	HORC	50.18598	12.49100	500
51	WB	JOC	50.21150	12.54840	510
52	WB	KOC	50.26417	12.23288	621
53	WB	KOPD	50.20319	12.47473	536
54	WB	KRC	50.33069	12.52950	806
55	WB	KVC	50.20496	12.51134	666
56	WB	NKC	50.23310	12.44790	564
57	WB	LAC	50.04967	12.62396	806
58	WB	LBC	50.26461	12.41123	684
59	WB	LOUD	50.27753	12.57449	692
60	WB	MAC	50.14429	12.53516	609
61	WB	POC	50.31997	12.42662	841
62	WB	POLD	50.15603	12.23497	589
63	WB	SKC	50.16911	12.36050	501
64	WB	STC	50.25794	12.51849	712
65	WB	TRC	50.30344	12.14466	612
66	WB	VAC	50.23450	12.37634	581
67	WB	ZHC	50.06984	12.30810	677

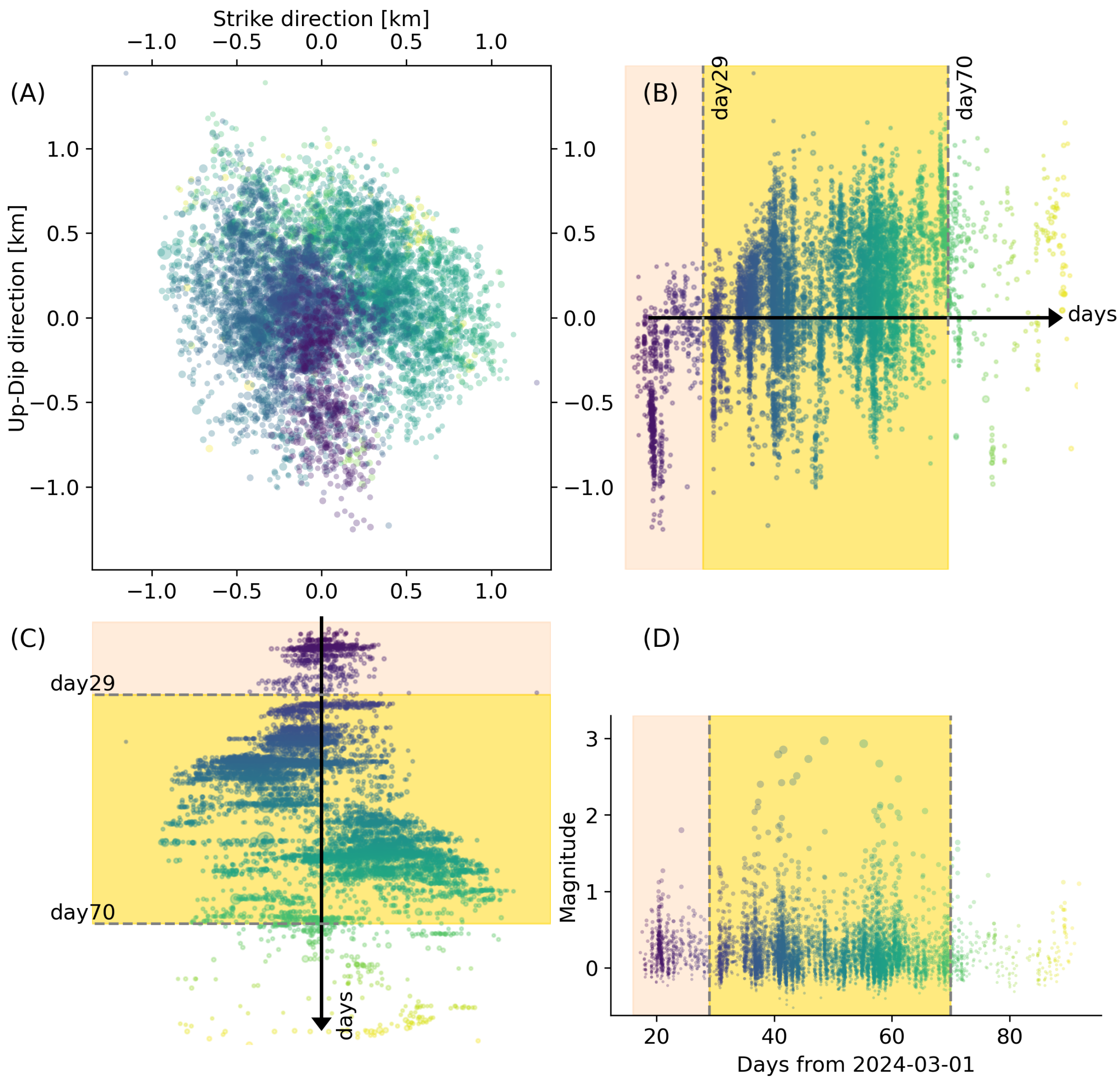

Fig. S2: Spatiotemporal and magnitude distribution of seismicity. (A) Hypocenter locations projected onto the fault plane, showing the up-dip versus strike directions. (B) Temporal evolution of events along the strike direction overlaid with highlighted time windows (pink and yellow shading indicate the days 1–28 and days 29–70 after March 1, 2024, respectively). (C) Temporal evolution of events along the up-dip direction, emphasizing the same time windows. (D) Magnitude distribution as a function of time, with the same highlighted intervals.

Double difference Wadati method for v_P/v_S ratio in source region of the swarm

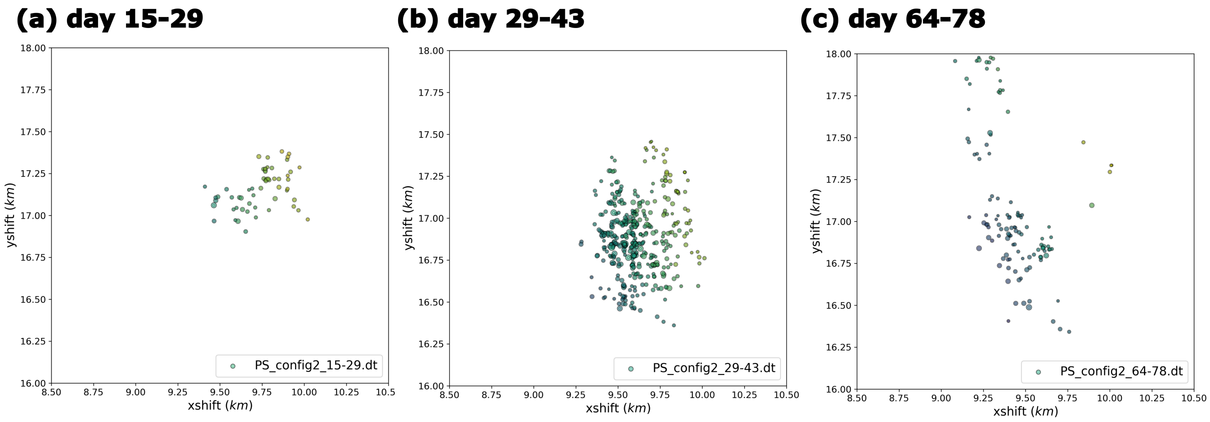

Fig. S3: Epicentral distribution of events considered in the double difference Wadati method (WadatiDD). All events were between 8 and 10 km depth. The panels a-c show the events that occurred during days 15-29, days 29-43, and days 64-78 after March 1, 2024.

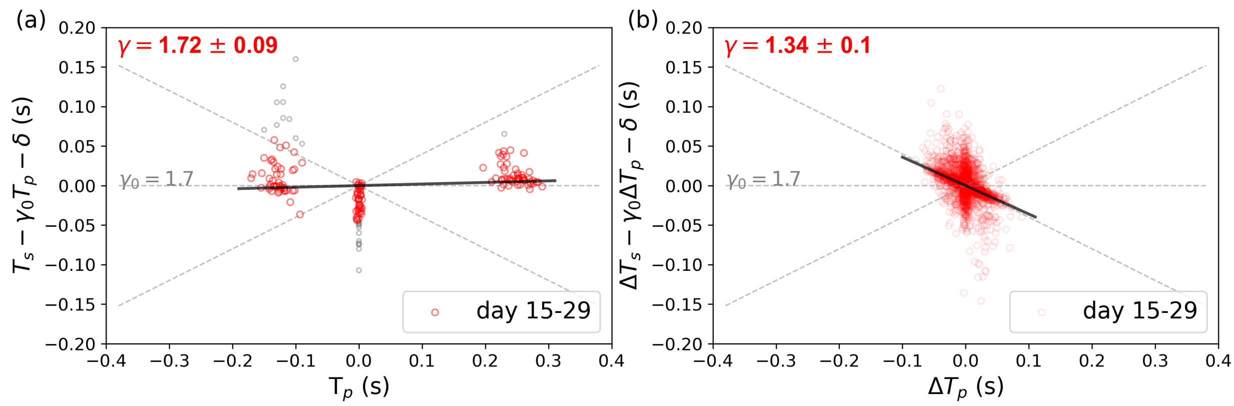

Fig. S4: Example of the regional (a) and source volume (b) WadatiDD plot for the time interval of days 15-27 after March 1, 2024. The vertical axis is reduced by a ratio of 1.7. The estimated velocity ratio $\gamma = v_P/v_S$ is annotated in red.

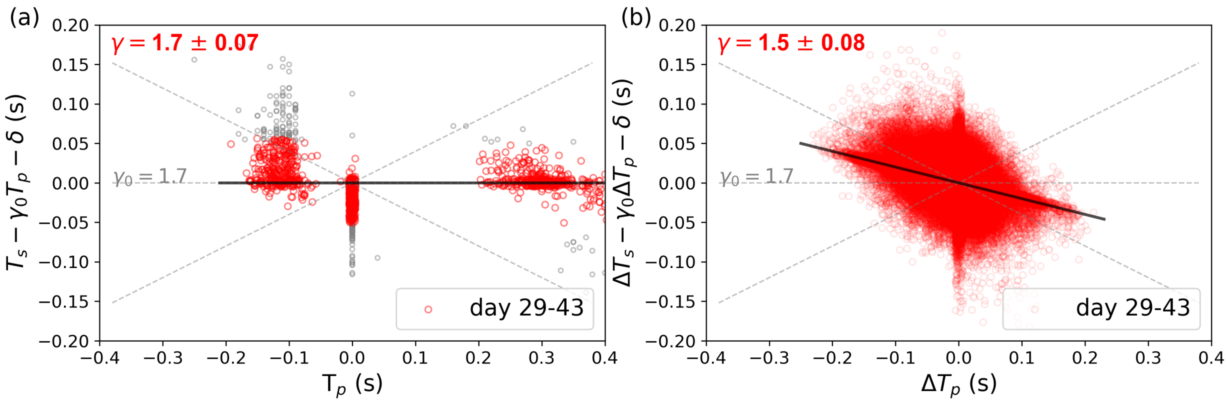

Fig. S5: Same as Fig. S4, but for the time interval of days 29-43 after March 1, 2024.

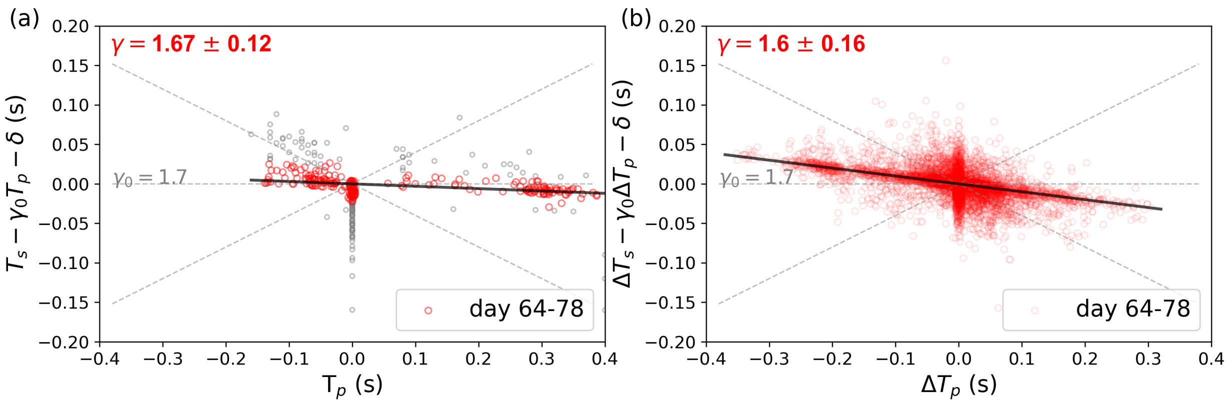

Fig. S6: Same as Fig. S4, but for the time interval of days 64-78 after March 1, 2024.

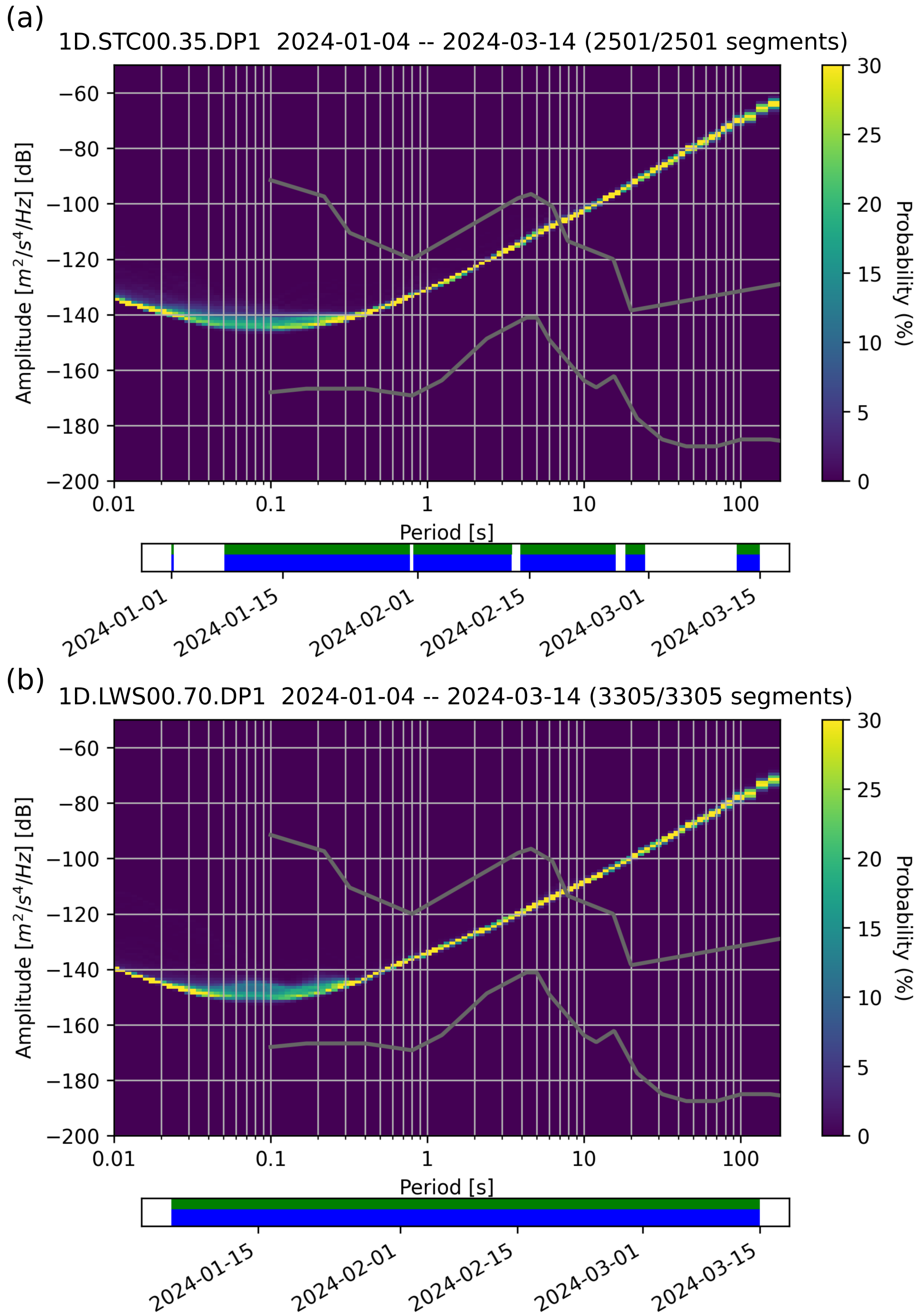

Fig. S7: Probability Power Spectral Density (PPSD) plots for borehole stations 1D.STC00.35.DP1 (depth: 353 m) and 1D.LWS00.70.DP1 (depth: 372.1 m), covering the period from 1 January to 14 March 2024, prior to the onset of the 2024 Klingenthal–Kraslice swarm. Both borehole stations exhibit high signal-to-noise ratios, as indicated by the low ambient noise levels in the PPSD. The figure shows the distribution of noise amplitudes as a function of period, with colors indicating the probability of occurrence.

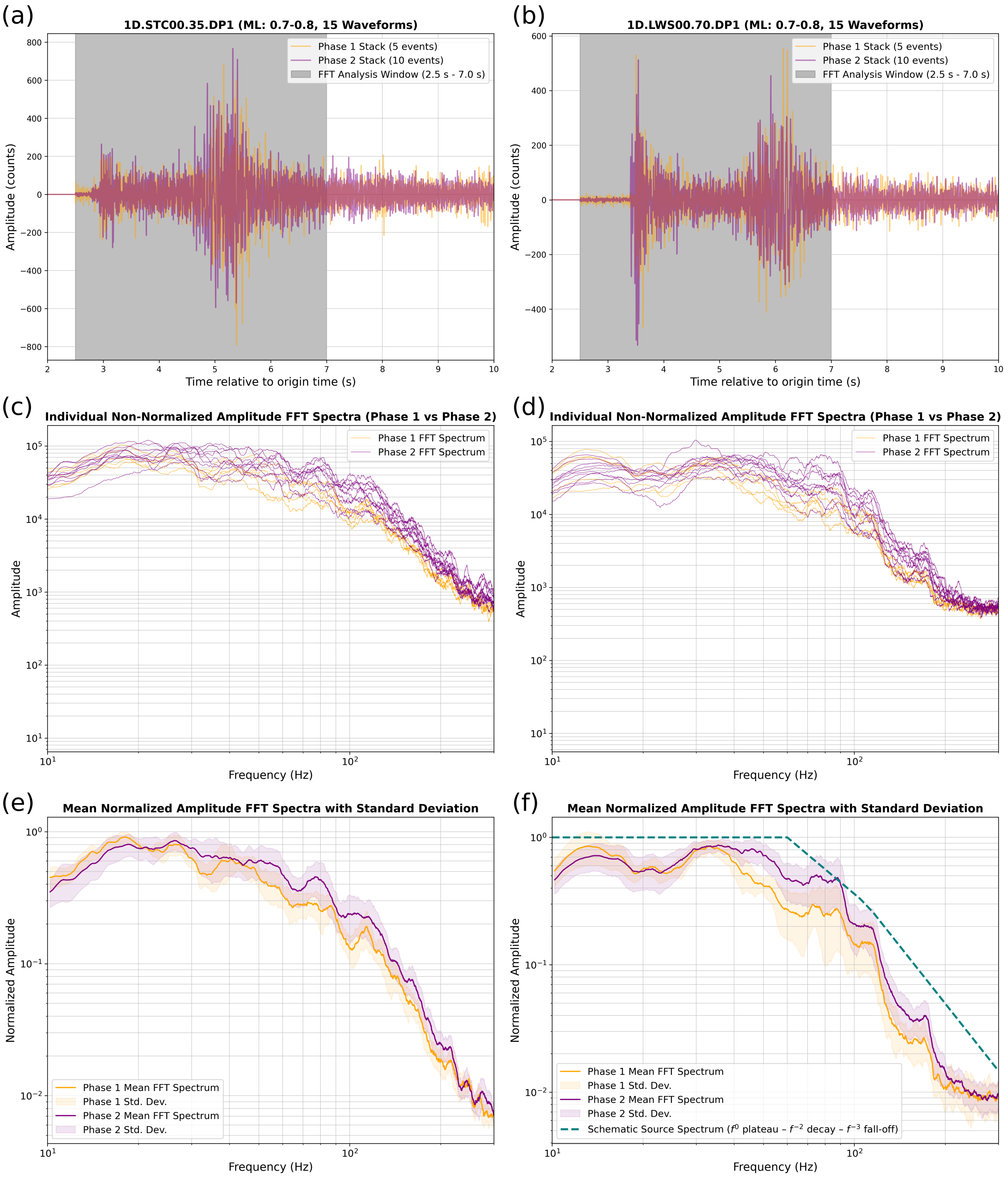

Fig. S8: Comparison of stacked waveforms and amplitude spectra for two borehole seismic stations: 1D.STC00.35.DP1 (Studenec, left column) and 1D.LWS00.70.DP1 (Landwüst, right column). All panels represent data for events with M_L 0.7–0.8. (a, b) Stacked vertical velocity waveforms aligned to origin time. The orange trace represents the stack of five events from Phase 1, and the purple trace represents the stack of ten events from Phase 2. The gray shaded region (2.5 s to 7.0 s after origin time) indicates the window used for Fast Fourier Transform (FFT) analysis. (c, d) Individual non-normalized amplitude FFT spectra comparing Phase 1 (orange) and Phase 2 (purple). Each thin line shows a single event's spectrum, illustrating event-to-event variability. (e, f) Mean normalized amplitude FFT spectra with standard deviation for Phase 1 (orange) and Phase 2 (purple). The dashed teal curve shows the schematic source spectrum, consisting of a low-frequency plateau (f^0), an intermediate f^{-2} decay, and a high-frequency f^{-3} fall-off, representing a generalized source spectrum for comparison.

Comparison of the 1897 and the 2024 Klingenthal–Kraslice swarms

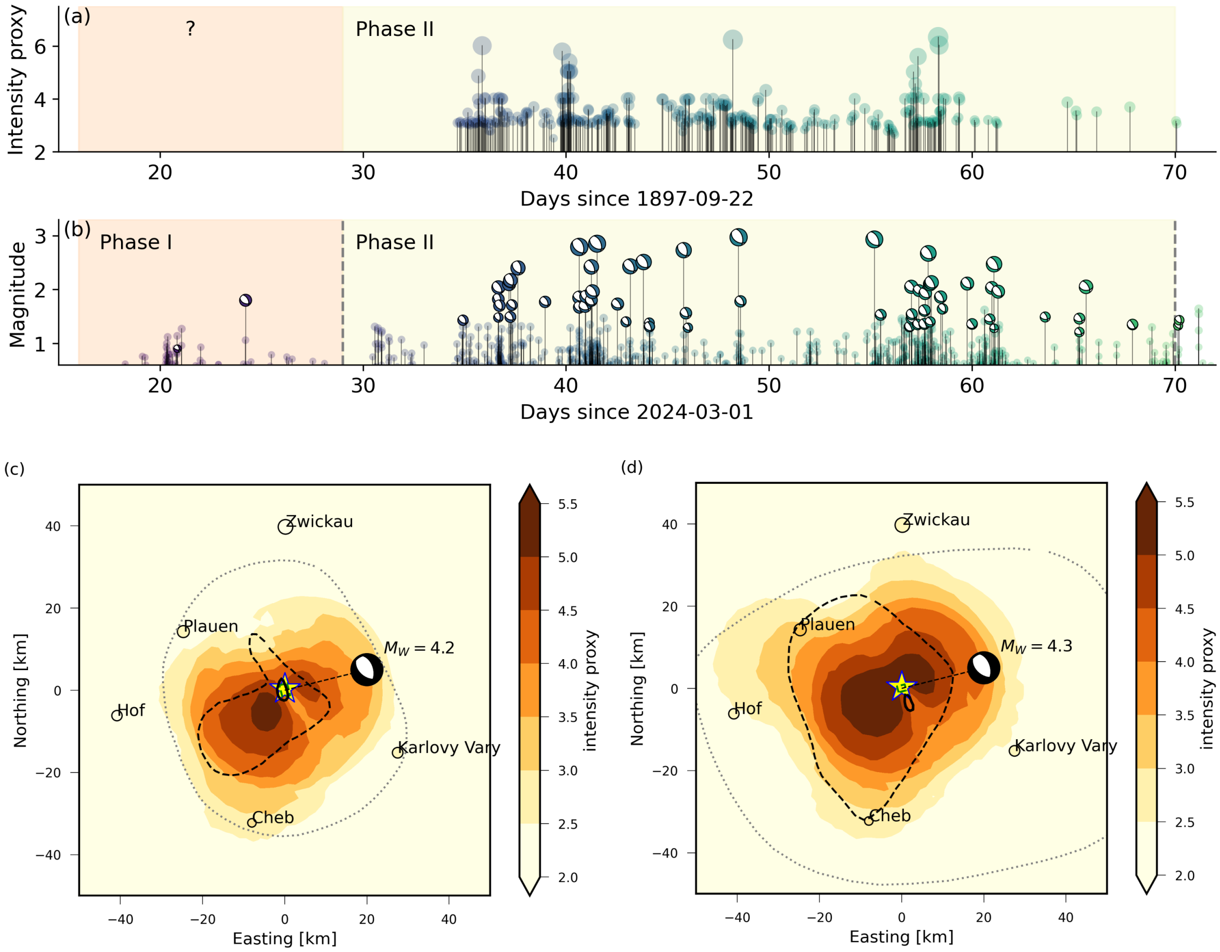

Fig. S9: Comparison of the seismicity and source parameters between the 1897 and 2024 Klingenthal–Kraslice swarms. (a) Events of the 1897 swarm plotted as a function of their occurrence in days. Strength is given by an intensity proxy, as defined in [e.g., 8]. (b) Magnitude over occurrence time of micro-earthquakes of the 2024 swarm. (c) Epicenter location and felt intensity of the October 29, 1897, M_W 4.2 Klingenthal earthquake. The hypocentre location and source mechanism of a M_W 2.5 earthquake from 2024 (see focal solution plot) were used to simulate intensities between 0.2 and 4 Hz. The contour lines show isoseisms of highly felt, felt, and poorly felt questionnaires. The dashed green lines show the geometry of the rectangular source used to simulate peak ground displacement (PGD). PGD was used to derive intensity proxies. (d) Similar as in (c), but simulating the November 7, 1897, M_W 4.3 Kraslice earthquake. Moment magnitudes were taken from [9, Table 3]. The mean epicentre location of the 2024 swarm is plotted by the yellow star. According to our simulations, the moment magnitude of the historical earthquakes could have been 4.2 and 4.3, respectively.

References

[1] Dahm, T., Ohrnberger, M., Vollmer, D., Woith, H. & Isken, M. Longterm monitoring of swarm earthquakes in the western eger rift (2024).

[2] Institute of Geophysics, Academy of Sciences of the Czech Republic. West bohemia local seismic network (1991). URL https://www.fdsn.org/networks/detail/WB/.

[3] Horalek, J., Fischer, T., Bouskova, A. & Jedlicka, P. Western Bohemia/Vogtland region in the light of the WEBNET network. Studia geoph. et geod. **44**, 107–124 (2000).

[4] University of Leipzig. Sxnet saxon seismic network (2001). URL https://www.fdsn.org/networks/detail/SX/.

[5] Institut fuer Geowissenschaften, Friedrich-Schiller-Universitaet Jena. Thüringer seismologisches netz (2009). URL https://www.fdsn.org/networks/detail/TH/.

[6] Department of Earth and Environmental Sciences, Geophysical Observatory, University of Munchen. Bayernnetz (2001). URL https://www.fdsn.org/networks/detail/BW/.

[7] Federal Institute for Geosciences and Natural Resources (BGR). Federal institute for geosciences and natural resources (2025). URL https://eida.bgr.de/.

[8] Credner, H. Die Sächsischen Erdbeben während der Jahre 1889 bis 1897, insbesondere das Böhmische Erdbeben vom 24. October bis 29. November 1897. Abh. Math.-Phys. Cl. K. Sächs. Ges. Wiss. **24**, 315–398 (1898).

[9] Dahm, T. et al. Seismicity in the block mountains between halle and leipzig, central germany: centroid moment tensors, ground motion simulation, and felt intensities of two M $\approx$ 3 earthquakes in 2015 and 2017. Journal of Seismology **22**, 985–1003 (2018). URL https://doi.org/10.1007/s10950-018-9746-9.